

# OSSE OBSERVATIONS OF THE CRAB PULSAR

M. P. Ulmer, S. Lomatch, S. M. Matz, D. A. Grabelsky, W. R. Purcell

Department of Physics and Astronomy, Northwestern University, Evanston IL 60208-3112

J. E. Grove, W. N. Johnson, R. L. Kinzer, J. D. Kurfess, M. S. Strickman

Code 7650, E. O. Hulburt Center for Space Research, Naval Research Lab,  
Washington D.C. 20375

R. A. Cameron<sup>1</sup>, G. V. Jung<sup>2</sup>

Universities Space Research Association Washington DC

Submitted to the Astrophysical Journal

Received 3 November 1993;    accepted 1 March 1994

---

<sup>1</sup>Present address, Harvard-Smithsonian CfA, Cambridge, MA 02138

<sup>2</sup>Postal address Code 7650, Naval Research Lab, Washington DC 20375

Report Documentation Page				Form Approved OMB No. 0704-0188	
Public reporting burden for the collection of information is estimated to average 1 hour per response, including the time for reviewing instructions, searching existing data sources, gathering and maintaining the data needed, and completing and reviewing the collection of information. Send comments regarding this burden estimate or any other aspect of this collection of information, including suggestions for reducing this burden, to Washington Headquarters Services, Directorate for Information Operations and Reports, 1215 Jefferson Davis Highway, Suite 1204, Arlington VA 22202-4302. Respondents should be aware that notwithstanding any other provision of law, no person shall be subject to a penalty for failing to comply with a collection of information if it does not display a currently valid OMB control number.					
1. REPORT DATE <b>1994</b>		2. REPORT TYPE		3. DATES COVERED	
4. TITLE AND SUBTITLE <b>OSSE Observations of the Crab Pulsar</b>				5a. CONTRACT NUMBER	
				5b. GRANT NUMBER	
				5c. PROGRAM ELEMENT NUMBER	
6. AUTHOR(S)				5d. PROJECT NUMBER	
				5e. TASK NUMBER	
				5f. WORK UNIT NUMBER	
7. PERFORMING ORGANIZATION NAME(S) AND ADDRESS(ES) <b>Naval Research Laboratory, Code 7650, 4555 Overlook Avenue, SW, Washington, DC, 20375</b>				8. PERFORMING ORGANIZATION REPORT NUMBER	
9. SPONSORING/MONITORING AGENCY NAME(S) AND ADDRESS(ES)				10. SPONSOR/MONITOR'S ACRONYM(S)	
				11. SPONSOR/MONITOR'S REPORT NUMBER(S)	
12. DISTRIBUTION/AVAILABILITY STATEMENT <b>Approved for public release; distribution unlimited.</b>					
13. SUPPLEMENTARY NOTES					
14. ABSTRACT					
15. SUBJECT TERMS					
16. SECURITY CLASSIFICATION OF:			17. LIMITATION OF ABSTRACT	18. NUMBER OF PAGES <b>46</b>	19a. NAME OF RESPONSIBLE PERSON
a. REPORT <b>unclassified</b>	b. ABSTRACT <b>unclassified</b>	c. THIS PAGE <b>unclassified</b>			

## ABSTRACT

We present results of the *Compton Gamma Ray Observatory OSSE* observations of the Crab pulsar, made during MJD 48373–48406 (27 April 1991–30 May 1991) and MJD 48798–48804 (25 June 1992–1 July 1992). Pulsar light curves and spectra over the  $\sim 0.05$  to 10 MeV range are presented. The arrival time of the gamma-ray peak and the radio peak agree to within  $30\mu\text{s}$ , which is better than the  $\sim 300\mu\text{s}$  accuracy of the measurements. The overall pulse phase averaged spectrum in the 0.1–10 MeV range is well-fit by a power law of the form  $0.05 \times (E/0.13 \text{ MeV})^{-(1.99 \pm 0.03)}$  photons  $\text{cm}^{-2} \text{ s}^{-1}$ . The outer-gap model (with gap parameter equal to 0.46) provided to us by Ho agrees with the data to better than 20%. The spectra of the bridge and second peak are slightly harder than the first peak as measured by the hardness ratio ( $\sim 110$ –220 keV)/( $\sim 50$ –105 keV):  $P1 = 0.54 \pm 0.01$ ,  $P2 = 0.63 \pm 0.01$ , bridge =  $0.68 \pm 0.03$ . The phase of the two peaks in the light curve is constant over the 50–550 keV range to within the accuracy of the measurements (better than 0.02 in phase). No evidence was found for variability of the light curve on time scales from 2 minutes (less than a factor of 1.8) to 1 year (less than a factor of 1.06), where these are  $3\sigma$  upper limits. However, when we examine the historical data base, we find, in agreement with Nolan et al., that there is evidence for a 13 year variation in the ratio of the intensity of peak 2 to peak 1. We show that if this is interpreted as being due to precession (which changes the relative view of the intrinsic gamma-ray pulse as seen on earth), the variation is consistent with models of neutron star structure. The optical data may be in conflict with the interpretation however. We found no statistically significant lines in the 50–550 keV range in the spectrum. The average  $3\sigma$  upper limits in  $10^{-3}$  photons  $\text{cm}^{-2} \text{ s}^{-1}$  for lines at 0.073, 0.078, 0.4, 0.44, 0.511, and 0.545 MeV are: 0.3, 0.5, 0.6, 0.5, 0.5, and 0.1. These limits are based on observations that spanned

approximately one week or more. Our results do not corroborate previous detections, most of which have been at the  $\sim 3\sigma$  level. We cannot exclude, however, the possibility of transient features with our current analysis.

## 1. INTRODUCTION

Despite many years of extensive study of the Crab pulsar, a detailed understanding of this object is still lacking, and a number of questions about its pulsed emission remain unanswered or open to debate. For example, Mahoney, Ling, & Jacobson (1984) found that the spectrum of the pulsed emission in the region between the two peaks has the same spectral shape in the 0.05 to 10 MeV range as do the pulse peaks, while others (e.g., Knight 1982 and Hasinger et al. 1984) suggest that the spectrum of the interpulse region is different. Numerous studies report the detection of lines or spectral features from the Crab nebula and pulsar (Leventhal, MacCallum, & Watts 1977; Ling et al. 1979; Strickman, Johnson, & Kurfess 1979; Ayre et al. 1983; Agrinier et al. 1990; Massaro et al. 1991, 1992; Manchanda et al. 1982; Gilfanov et al. 1994). In contrast, many other observations have failed to detect these lines (Mahoney et al. 1984; Ling et al. 1977; Schwartz et al. 1980; Hameury et al. 1983; Knight 1982; Hasinger et al. 1982).

There have also been reports that the ratio of counts in the two pulse peaks, at energies  $\geq 50$  MeV, varies with time (Clear et al. 1987; Nolan et al. 1993; Kanbach 1990). Previous tests for time variability in the 100 keV range, based on comparisons of light curves, have spanned time scales of less than 10 years (Toor & Seward 1977; Mahoney et al. 1984; Hasinger et al. 1984). A study similar in time duration, detail, and method as the high-energy ones has not been carried out at gamma-ray energies of  $\sim 100$  keV.

In this paper, we report on observations of the Crab pulsar made with the Oriented Scintillation Spectrometer Experiment (OSSE) on the *Compton Gamma Ray Observatory*. The large area of OSSE (2000 cm<sup>2</sup> at .511 MeV) and the long observing time we obtained for the Crab pulsar ( $\sim 3$  weeks) represent a significant increase in sensitivity in the .05–10 MeV energy range over previously flown experiments, making our measurements of the pulse shape and spectrum the most sensitive to date. In §2 we describe the observations.

Our analysis and results, including the timing analysis, light curves, and energy spectra, are discussed in §3. In §4 the OSSE results are discussed in the context of previous studies of the Crab pulsar. A summary and conclusions are presented in §5.

## 2. OBSERVATIONS

The Oriented Scintillation Spectrometer Experiment is one of four gamma-ray instruments on the *Compton Gamma Ray Observatory* (Johnson et al. 1993; Ulmer et al. 1993). OSSE consists of 4 identical NaI(Tl)/CsI(Na) phoswich detectors with sensitivity in the .05–10 MeV energy range. The field of view of each detector is  $11.4^\circ \times 3.8^\circ$  (FWHM response), defined by a tungsten slat collimator. Each detector can be independently rotated about a fixed axis which is parallel to the long direction of the collimator (and the spacecraft y-axis). Energy losses in each phoswich detector are measured and recorded for later transmission to the ground, along with instrument configuration information and other housekeeping data.

For typical spectral observations, detectors alternately observe source and background positions roughly every two minutes in order to obtain local background measurements. For analysis of pulsed emission, however, only the on-source positions are used. OSSE pulsar modes permit transmission of time-tagged gamma-ray energy losses. Because the entire event stream for all four detectors cannot be accommodated in OSSE’s portion of the satellite telemetry, the pulsar processing includes event selection and compression for telemetry formatting. Up to eight energy-band definitions may be included in the transmitted pulsar data. These energy bands, as well as the rest of the pulsar data collection configuration, can be defined by OSSE mission operations activities and uploaded to the instrument via command. The pulsar data acquisition can therefore be optimized to the specific observing strategy and energy range of particular interest, while limiting the event rate to that which can be accommodated by the OSSE telemetry.

Gamma-ray events qualified as being in one of these eight energy bands are processed onboard in one of two modes: (1) event-by-event (EBE) mode, where selected events are time-tagged, and both energy loss and arrival time at the spacecraft are transmitted in the telemetry; or (2) rate mode, where high time resolution rate samples are taken in each of the eight energy bands.

The EBE mode data provide the highest time resolution, and are therefore suited for the study of fast pulsars. Events are time-tagged with a resolution selectable from either 0.125 or 1 milliseconds. In this mode, spacecraft arrival times, detector identifications, and encoded energy losses are transmitted. At the highest resolution, the telemetry bandwidth supports a maximum event rate of  $\sim 290$  events per second. Regardless of the resolution selected for telemetry, gamma-ray events that pass the instrument anti-coincidence criteria (valid gamma-ray events) are registered on board the spacecraft with 1/8 millisecond ticks, relative to the UTC time marking the beginning of each standard 2.048 s data packet. Event timing precision in the telemetry stream may then be truncated, depending upon the selected resolution.

The pulsar rate mode can accommodate a much higher event rate, but at the expense of spectral resolution. This mode records the number of events in each of the defined energy bands at a specified sample frequency. The highest sample rate in this mode provides a resolution of 4 milliseconds. Sample times from 4 msec to 512 msec can be selected. In this mode OSSE can achieve its best sensitivity to a continuum flux.

The data we present here were collected in the 1 millisecond EBE mode and 1/8 millisecond EBE mode. The energy ranges and detectors used were varied over the course of the observations to allow approximately full coverage of the energy range of the OSSE instrument, and optimal use of the telemetry band width and inherent detector sensitivity. Table 1 gives the times, energy ranges, and timing precisions of the OSSE observations of the Crab. We achieved overall spectral coverage and good sensitivity, although we did not

achieve the maximum sensitivity possible in any one energy range. Because a study of the source 1A 0535+262 was included in the Crab observation plan, the detectors were not always pointed directly at the Crab pulsar. In terms of pointing the OSSE collimator at the Crab pulsar, the coverage was 50% optimal for the observations covering TJD 8373–8377 and 8393–8400, and 25% for the remaining days. The net  $\text{cm}^{-2} \text{s}^{-1}$  accumulated was about  $6 \times 10^7 \text{ cm}^{-2} \text{s}^{-1}$  for energies below about 520 keV.

### 3. ANALYSIS AND RESULTS

#### 3.1. TIMING

OSSE standard pulsar analysis has been described in Ulmer et al. (1993). Briefly, we epoch-folded the data using the relative phases of these events according to the following formula, which converts the arrival time at the solar system barycenter to a phase:

$$\phi(t) = \phi(t_0) + \nu_0(t - t_0) + \dot{\nu}_0(t - t_0)^2/2 + \ddot{\nu}_0(t - t_0)^3/6. \quad (1)$$

The value of  $t_0$  is, by convention, the integer portion of the TJD specifying the radio pulse used to define the ephemeris. To compare the radio pulse arrival time to that of the gamma rays, we use the value of the arrival time at the geocenter of the first radio pulse after the beginning of  $t_0$ . The time of this first pulse, referred to as  $t_{0\text{geo}}$ , is converted to arrival time at the solar system barycenter (SSB), and its phase is derived using Equation 1. All UTC arrival times are corrected to the SSB using the JPL DE200 planetary ephemeris (E. M. Standish 1989, private communication), and standard GRO software derived from the radio pulsar processing program TEMPO (Taylor & Weisberg 1989). Radio arrival times correspond to infinite frequency, and have been corrected for dispersion effects. Since the dispersion measure of the Crab is variable (Agrinier et al. 1990, and references therein),

simultaneous dispersion measurements are required to achieve accuracy exceeding  $300\mu\text{s}$ . The pulsar parameters used in our timing analysis, derived from the radio ephemeris provided by Arzoumanian, Nice, & Taylor (1992), are listed in Table 2; also listed are the values of dispersion measures used in the analysis of the radio data.

### 3.2. LIGHT CURVE

#### 3.2.1. PROFILE FITS

Because the GRO clock is stable to better than  $\sim 100\mu\text{s}$  (based on spacecraft timing studies), we were able to bin the data of our most sensitive energy range into 256 phase bins and obtain the maximum time resolution. The resultant light curve is shown in Figure 1. In order to avoid oversampling the data, we used only the  $1/8$  ms time-tagged data to produce this light curve. However, we tested for the effect of a slight amount of oversampling in the light curve by epoch-folding 1 ms data from another OSSE observation over 64 phase bins. Within the uncertainties, the measured separation of the two pulse peaks in the oversampled, 1-ms light curve was the same as that in the  $1/8$  ms light curve.

At energies above about 200 keV, the signal-to-noise ratio is not high enough to warrant folding the data over phase bins narrower than  $\sim 1$  ms. Light curves from 1 ms time-tagged data in 5 energy ranges are shown in Figure 2. The data have been oversampled by a factor of 2 for the first three energy ranges, spanning 0.05–0.55 MeV, and undersampled (due to poor statistics) in the highest energy range of 0.52–9.7 MeV. At all energies where the pulse is evident, the light curves are characterized by two peaks, referred to as “P1” and “P2,” plus a region between the peaks, referred to as the “bridge.”

We attempted to fit the entire light curve in Figure 1 with a modified asymmetric Lorentzian profile, following Hasinger (1984b), and Hasinger et al. (1984). In this model

the region between the two peaks is represented by the functional form.

The functional form that we used to describe the left side of each peak plus background is:

$$f(x) = \frac{\alpha}{1 + \left(\frac{\beta-x}{\gamma}\right)^\delta} + \varepsilon \quad ; \quad (2)$$

where  $\beta$  defines the phase on the peak,  $\gamma$  and  $\alpha$  are the peak half widths and amplitudes,  $x$  is the phase at which the function is evaluated,  $\delta$  determines the slope, and  $\varepsilon$  is the background term. For the right side of each peak the term with  $\beta$  and  $\gamma$  changes to  $(x - \beta)/\gamma$ .

Fitting such a functional form to the entire observed light curve can provide empirical information about the gamma-ray emission regions of the pulsar, but we could not obtain statistically acceptable fits of this model to our  $\sim 50$ – $220$  keV data. Regardless of the initial parameter values used (including those of Hasinger et al. 1984), all of the  $\chi^2$  probabilities we obtained with this model were less than  $10^{-6}$ .

In the above form,  $\delta$  was kept the same for both peaks, however if we allow  $\delta$  to be different for each peak, we can at least describe the peaks and bridge region to typically better than 20%. This fit (given below) to the 1/8 millisecond data in Figure 1 can be used especially by those who desire an analytic form to approximate the peaks and their sharpness. The values for our best fit were: for peak 1,  $\beta = 0.99$ ,  $\gamma$  left side = 0.023,  $\gamma$  right side = 0.028,  $\alpha = 6.1$ , and  $\delta = 1.30$ ; and for peak 2,  $\beta = .40$ ,  $\gamma$  right side = 0.064,  $\gamma$  left side = 0.018,  $\alpha = 8.1$ , and  $\delta = 1.17$ ; the background was 25.1 and the chi-squared (246 degrees of freedom) = 341. The fit was made by fitting each peak individually over  $\pm 0.05$  in phase about each peak. Then, these results were combined to produce a function over the entire 0 to 1 phase range. As noted above the function does describe the peaks (chi-squared probabilities for obtaining a larger value if the model for the peak alone is correct are 0.04 and 0.7 for peaks 1 and 2) and bridge, but where this function has the largest percentage discrepancy with the data is the background region (phase 0.45 to 0.9)

as the function predicts a non-zero flux (above the background) in this region.

In the above model, a precise determination at the peak phase bin is not possible as the freedom to change the slope of each side of the peak allows for a large ( $\sim 0.05$ ) variance in the value for the peak phase bin. But, by using only the pulse-peak regions of the light curve, we were able to obtain acceptable fits using a simple Gaussian profile, and thereby determine the centroid of the peak positions from the fits. The results for several energy ranges are shown in Figure 3. The fit to the 1/8 ms data in the  $\sim 50$ –110 keV energy range yielded the most precise position, giving a phase of  $0.9992 \pm 0.0008$  for the first peak, where the radio phase for this peak is, by definition, 1. This corresponds to agreement with the radio phase of  $\lesssim 30 \pm 30 \mu\text{s}$ , and exceeds the quoted accuracy for the absolute phase of the radio pulse ( $300 \mu\text{s}$ ) and the timing accuracy of our experiment  $\sim 125 \mu\text{s}$ .

### 3.2.2. TIME VARIABILITY

We searched for time variability of the light curve intensity on time scales ranging from two minutes to three weeks. For the longer time scales we produced light curves with 64 phase bins, which corresponds to oversampling the data by approximately a factor of 2. However, because the statistics are somewhat marginal on two-minute time scales (e.g., the pulse is only evident in the average 2 minute light curves at the  $\sim 3$ – $5\sigma$  level), light curves with 32 phase bins were used for the short time-scale searches. Data covering  $\sim 50$ –340 keV were used to optimize the combination of large energy range and signal-to-noise. Data from each detector were analyzed separately.

The method employed was designed to measure scaling deviations of a test profile,  $y$ , from a template profile,  $x$ , as given by a least-squares fit to the function

$$y_i = A + Bx_i \quad (i = 1, \dots, n \text{ phase bins}).$$

The parameter  $B$  provides a measure of scaling deviation of  $y$  from  $x$ , with values significantly different from 1 indicating variability. For the short time scale study,  $x$  is taken to be a single, high-statistics, average profile, while  $y$  represents any one of the individual, short time scale light curves in the average. The least-squares fit is performed for each  $y$ , with the assumption that the correlation between  $y$  and  $x$  is negligible, owing to the large number of short time scale profiles averaged together to produce  $x$ . In this case, the relevant  $\chi^2$  statistic and the parameter errors  $\sigma_A$  and  $\sigma_B$  yield their standard statistical interpretation. For the long time scale study,  $x$  and  $y$  are both high signal-to-noise light curves, representing large scale averages from different observation periods.

For this test, the  $\chi^2$  statistic is taken to be the most general form of

$$\chi^{2'} = \sum_{i=1}^n \frac{(y_i - A - Bx_i)^2}{(\sigma_{y_i}^2 + B^2\sigma_{x_i}^2)}. \quad (3)$$

In the short time scale case, we have  $\sigma_{x_i}^2 \ll \sigma_{y_i}^2$ , and the second term in the denominator of equation 3 can be neglected. In addition to  $\chi^2$ , this procedure also yields estimated uncertainties to the best-fit values for  $A$  and  $B$ . As a confirmation that the uncertainties to  $A$  and  $B$  are valid, we note that the average assigned errors agree to within about 10% of the standard deviation of the distribution of the computed values of  $A$  and  $B$ .

The results of this investigation showed no evidence for variability on any time scale. Table 3 contains  $3\sigma$  confidence limits on variability in the light curve for different time scales from several observations. The limits correspond to 3 times the average deviation of  $B$  from the mean. In all cases, the  $\chi^2$  values obtained indicated acceptable fits.

### 3.3. SPECTRAL ANALYSIS

#### 3.3.1. CONTINUUM

In order to perform phase resolved spectral analysis of the data, we had to distinguish the phase portions of the light curve which represent source plus background from those which represent only background. “Background” includes unpulsed emission from the pulsar (if any) and emission from the Crab nebula, as well as detector background. The background portion was then subtracted from the entire light curve. The phase ranges we have defined for each component (the two peaks, the bridge, and the nebular/local background) are listed in Table 4. These ranges were chosen based on the shape of the light pulse profile in the range  $\sim 50\text{--}220$  keV, and are consistent with previous definitions of these 3 regions (cf., Wills et al. 1982; Walraven et al. 1975; Kurfess 1971; Massaro et al. 1991, 1992; Knight 1982; Mahoney et al. 1984). To test for the dependence of our results on the choice of background phase bins, we varied the range by up to 3 phase bins on either side of our standard range. No statistically significant change in our results could be detected for this variation, and we therefore only present results for those phase-bin regions given in Table 4. Note that for the spectral fits for peak 1, peak 2, bridge and total pulse, we quote the phase averaged normalization, e.g., the instantaneous intensity for peak 1 was multiplied by 0.1 (cf. the phase intervals in Table 4).

We fit single and double (broken) power law spectral models to our data using a standard forward folding technique. The model photon spectrum is folded through the OSSE instrument response to produce a model count spectrum, which is compared to the measured count spectrum. The parameters of the model photon spectrum are adjusted iteratively so as to achieve a (least-squares) best-fit of the model count spectrum to the measured count spectrum. For the single power law, the uncertainties to the best-fit parameters of each photon spectral model were estimated by the increment to the spectral index required to yield a  $\chi^2$  equal to  $\chi^2_{min} + 1$ , and the uncertainties in the normalization are based on our estimate of our 90% confidence uncertainty in absolute calibration of 5%. As the broken power law fits are not a statistically significant improvement over the single power law fits, we do not quote uncertainties here for the parameters to the best fits to the

broken power law models (see also §4.3.2).

Best-fit parameter values for the single and broken power law models are given in Tables 5 and 6. Figures 4a,b,c show the spectra along with best fits for the two peaks and bridge regions. Both models produced acceptable fits, with no statistically significant improvement of broken power law compared to the single power law. Evidently, we cannot use our data alone to distinguish between these two models. See also §4.3.2, where we combine our results with those previous experiments at lower energies.

The single power law model was also fit in several narrow phase ranges (0.08 of a Crab period) across the pulsed emission region from 0.85 to 0.55 in phase. The resulting power law index in each range, shown in Figure 5, does not appear to display significant evidence of spectral variation with phase. (Again, we will discuss this result further in §4.)

We also investigated the dependence of spectral shape on pulse phase by computing several hardness ratios as a function of pulse phase. While this method is not diagnostic of specific spectral features, it does not suffer from the limited statistics per energy and phase bin inherent in the spectral fits over narrow phase ranges. The results, shown in Figure 6, indicate no significant variation of hardness with phase with the exception of the ratio of (110–220 keV)/(50–105 keV). In all other cases, a constant provided an acceptable fit to each hardness–phase plot. The effect for the (110–220 keV)/(50–105 keV) ratio is formally  $5\sigma$  ( $\chi^2 = 103$  for 47 degrees of freedom). We can examine this effect further by averaging the (110–220 keV)/(50–105 keV) hardness ratio in phase over the P1, P2 and the bridge. Then we find the following values for this ratio:  $0.54 \pm 0.01$  for P1,  $0.63 \pm 0.01$  for P2, and  $0.68 \pm 0.03$  for the bridge. We note that the broken power law model fit to the OSSE data has its break at about 110 keV, so this hardness ratio compares the fluxes above and below the break, and hence might be expected to be most sensitive to overall changes in spectral shape.

### 3.3.2. *LINES*

To search for line features in our data, the background-subtracted count rate spectra were accumulated over 1 to 2 week intervals, and averaged over the phase intervals defining the bridge and peak regions, and separately over the total light curve (cf., Table 4). The search for transient features that could have occurred on time scales of days or less will be the subject of a future paper.

We performed fits to our data by modeling narrow lines at both the fixed energies reported by previous studies (see Table 7), and within energy ranges where deviations from the continuum were apparent by inspection. The line widths reported in the literature are all consistent with being “narrow lines,” i.e. significantly narrower than the detector energy resolution. We therefore fixed the widths in our models so that all features were consistent with the OSSE energy resolution. Also, because only emission lines have been reported, we constrained the line fluxes in our models to be positive. The results are presented in Table 7.

No lines were detected with a significance greater than  $3\sigma$ , where the uncertainty ( $\sigma$ ) represents the increment to the best-fit line flux that gives a  $\chi^2$  of  $\chi^2_{min} + 1$ . For each line, the upper limits given in Table 7 correspond to  $3\sigma$  plus the best-fit line flux value. Neither relaxing the constraints on the widths of the lines in the model to allow for line widths up to twice the instrument resolution, nor allowing for absorption features in the model, resulted in any statistically significant lines. The upper limits obtained from the less constrained models were the same as those given in Table 7. Thus the uncertainties listed provide a good measure of the OSSE sensitivity to line emission in a pulsed source (for the net exposure, see §2) to both absorption and emission lines with widths from one to two times the instrument resolution.

## 4. DISCUSSION

The OSSE data have permitted a thorough analysis of the Crab pulsar spectrum and pulse shape, with optimal sensitivity obtained in the 50 to 500 keV energy range. These results will now be discussed in the context of previous work on the Crab.

### 4.1. PULSE SHAPE

Based on fits of a modified Lorentzian profile to Crab pulsar light curves from several hard X-ray/low energy gamma-ray observations (near 100 keV), Hasinger et al. (1984) argued that the bridge region is a simple superposition of the pulsar beam patterns that produce the two peaks in the light curve. We have found, with improved statistics, that this model does not describe the pulse profile derived from the OSSE data in the  $\sim 100$  keV range. A poor fit with a modified Lorentzian does not rule out the basic concept of beam superposition proposed by Hasinger et al., however, because the pulsar mechanism itself is not well enough understood to predict beam patterns and their expected energy and phase dependence.

One of the most striking characteristics of the Crab light curve is the apparent energy-independence of the phase of the peaks. The alignment of the radio and gamma-ray phases to within  $300\mu\text{s}$ , described in the previous section, is in good agreement with the work of Mahoney et al. (1984). The constant phase separation between peaks 1 and 2 with energy (cf., Figure 3) has been suggested by Ulmer et al. (1993) to be evidence for phase-locked pulsations in the gamma-ray region, which is produced by non-thermal emission processes. Such a hypothesis is consistent with theoretical interpretations of the spectral shape of the Crab pulsar, in which the gamma-ray emission is non-thermal in origin (cf. Cheng, Ho, & Ruderman 1986a,b; Daugherty & Harding 1982; Arons 1984; Ho 1993; Chiang & Romani 1993, and references therein). For other pulsars such as Vela

(Ögelman, Finley, & Zimmermann 1993), the soft X-ray flux is possibly dominated by thermal emission, hence the distinction here between thermal and non-thermal processes.

## 4.2. TIME VARIABILITY

Pulsed emission from the Crab is well known to be highly variable in intensity at radio wavelengths (Lundgren et al. 1992, and references therein). By contrast, in the optical bands the pulsar is remarkably stable, with variations being less than about 1% (Kristian 1971; Jones, Smith, & Nelson 1980). The results of our search using the OSSE  $\sim 100$  keV data failed to reveal any significant variability in the pulsed emission. This is consistent with the lack of variability seen in the optical range on the time scale of several weeks. A direct search for enhanced pulsed emission in the gamma rays coincident with the giant radio bursts also yielded a null result (Lundgren et al. 1994).

An intriguing variation in the intensity of the two peaks has been reported by Kanbach (1990), and by Nolan et al. (1993); these results show that the ratio of intensity of P1 to P2 appears to vary sinusoidally, with a period of about 13.5 years. Their analyses included data from SAS II, COS-B, and EGRET, and utilized a consistent set of phase conventions for the peaks (cf., Clear et al. 1987). Mahoney et al. (1984) concluded that the peak intensity ratio *did not* vary systematically with time, but they did not use a consistent set of phase conventions when analyzing the data from different experiments. With our OSSE data, we have extended the time baseline for this study at energies below  $\sim 1$  MeV to roughly 20 years.

The fits to the two separate energy ranges are statistically consistent with each other, giving a period of  $13.5 \pm 0.4$  yr in the high energy range, and  $12.9 \pm 0.5$  yr in the low energy range. With the assumption that the effect in both energy ranges is real, and tied to a common physical mechanism (e.g., precession), we fit both ranges simultaneously, with

the constraint that the frequency and phase of the two sinusoids be the same. In this case we obtained a period of  $13.1 \pm 0.1$ . We note that in both energy ranges, we can rule out the possibility that the observed variations are random fluctuations about the weighted mean; this conclusion has a  $3.3\sigma$  confidence level above 50 MeV, and a  $4\sigma$  confidence level in the 50–400 keV range. Figure 7 shows the simultaneous fit of a sinusoid to data in the 50–400 keV range and to data above  $\sim 50$  MeV.

Kanbach (1990) argued that a period of  $\sim 13$  years is consistent with neutron star precession caused by magnetic dipole induced moment differences or crust rigidity effects. Similarly, L. S. Finn (1993, private communication) has shown that this period is consistent with free precession of a neutron star if reasonable assumptions are made about the equation of state. However, while these results are suggestive, the lack of source variations larger than 1% at optical wavelengths (Jones et al. 1980) over  $\sim 10$  year time scale may impose complicated requirements on any precession model. Clearly, more observations are needed, along with a careful analysis of data in all wavebands, in order to evaluate this interesting and potentially revealing effect.

### 4.3. SPECTRA

#### 4.3.1. LINES

There have been nearly as many reports of detections of lines from the Crab pulsar as upper limits that conflict with the claimed detections (cf. references in Table 7 and §1). Similar disagreement can be found in the theoretical arena. For example, Massaro et al. (1991, 1992) presented a case for detectable flux from positron annihilation near the neutron star surface, while Arons (1983a) argued the opposite. The difference between these two predictions is in large part due to the assumptions about the beaming of this annihilation radiation. Similarly, the energy and strength of cyclotron lines is also an open

question (see, for example, Brecher & Ulmer 1978; Arons 1983b; Ho 1993, and references therein). This ambiguity prevents substantive conclusions from being made about pulsar models based on the non-detection of lines.

In §3 we concluded that none of the previously reported lines were detected by OSSE. Our upper limits between 50 and 550 keV apply even at energies besides those at which previous detections have been reported. Our results and the comparison with earlier work, presented in Table 7, also include two cases which were not obviously pulsed (Manchanda et al. 1982; Gilfanov et al. 1994). Except for the relatively low flux level reported by Massaro et al. (1991) we are in apparent disagreement with these detections. But as all of these detections are near the  $3\sigma$  level this disagreement is not large. Furthermore, it can't be ruled out that variable emission (on time scales of hours to a few days) from the Crab was either missed or averaged over by the OSSE observations.

#### 4.3.2. *CONTINUUM*

In order to better determine the shape of the pulsar spectrum, we have used lower energy data from previous experiments. As the data overlapped a great deal, we simply fit the OSSE data combined with the OSO-8 data (Pravdo & Serlemitsos 1981). But, as can be seen in Figure 8, the data from two other experiments (Fritz et al. 1971; Toor & Seward 1977) agree well with the OSO-8 data. Here we do not report a detailed comparison with the other CGRO experiments as this will be provided in a future paper. As elsewhere in this paper the pulse intensity is averaged over the entire pulsar cycle.

First we consider the outer-gap model of Ho (1989, 1993), and Cheng et al. (1986a,b). This is the only model of which we are aware that makes a prediction of the spectral shape in the OSSE energy range. We have fitted the model provided by C. Ho (1992, private communication) to the combined OSSE and OSO-8 data. The best fit, shown in Figure 8,

was  $0.46 \pm 0.06$  for the gap parameter ( $\chi^2 = 57$ , 24 degrees of freedom), in good agreement with the value quoted by Ho (1989). Unlike Ho (1989, 1993) however, we included a normalization to optimize the best fit. The best-fit for this normalization was  $0.86 \pm 0.03$ . Under the best of circumstances, the outer-gap model predicts the total intensity as well as spectral shape, and we see here that the model did indeed predict the intensity to within 14%; i.e., the normalization factor for our data is 0.86 rather than 1.0. Formally, the value of  $\chi^2$  is not good, but given the uncertainty in normalization (estimated to be between 5 and 10%) when combining the OSO-8 and OSSE data, the fit we obtained can be considered a valid description of the data to better than 20%.

Next, we discuss the power law fits to the data. The results of these fits and the fits to lower energy data with simple power laws and broken power laws are shown in Figure 8. A broken power law  $[0.062 \times (E/0.125 \text{ MeV})^\alpha \text{ photons cm}^{-2} \text{ s}^{-1} \text{ MeV}^{-1}]$  where  $\alpha = -1.84$  for  $E \leq 0.125 \text{ MeV}$  and  $-2.09$  for  $E > 0.125 \text{ MeV}$ ;  $\chi^2 = 16$ , 22 degrees of freedom] is formally only slightly favored over a single power law  $[(0.100 \pm 0.005) \times (E/0.094 \text{ MeV})^{1.87 \pm 0.02} \text{ photons cm}^{-2} \text{ s}^{-1} \text{ MeV}^{-1}]$ ,  $\chi^2 = 25$ , 24 degrees of freedom] fit to the OSO-8 and OSSE data combined.

The uncertainties for the parameters for the single power law were derived as discussed in §3.3.1. For the case of the broken power law, we have 3 parameters that are correlated with each other: the “break energy” is correlated with the indices above and below the break. To make an estimate of the uncertainty of the break energy, we produced equal value  $\chi^2$  contour maps of  $\alpha_i$  versus  $E_b$ , where  $\alpha_i$  is the index above or below the break energy ( $E_b$ ). For all of these cases, we assumed there were two “interesting” (cf. Avni 1976) parameters, which were those for which the chi-squared contour maps were being made. All the other parameters were left floating. Both maps produced limits to the break energy that were the same to within  $\sim 10\%$ ; the 90% confidence range for the break energy being 0.08 to 0.2 MeV. We also produced  $\chi^2$  contour maps for the spectral indices. The 90% confidence range is: for the lower energy spectral index  $-1.8$  to  $-1.9$ ; and, for the higher

energy spectral index range  $-1.9$  to  $-2.4$ .

We have made a careful comparison of the data from the 4 independent OSSE detectors and find that the individual spectra agree to better than 5%. But, the differences that are observed do not affect the spectral shape in our energy range. We have also shown that there is no statistically significant difference between the spectral shapes derived for variations within 1 standard deviation of the best estimates for our photo-peak efficiency. We therefore conclude that any systematic effects in our data do not affect our conclusions about the spectral shape.

Mahoney et al. (1984) suggested that no break exists in the  $\sim 50$ – $550$  keV range. We find agreement with this result when we restrict analysis to the OSSE data alone. Knight (1982, 1983), whose data spanned the  $\sim 20$  keV to 1 MeV range, did find a break at 39 keV in contrast to our finding that the break energy is near 125 keV. Given the lower statistical significance of the Knight (1982) data in the  $\gtrsim 100$  keV range, this disagreement is not serious. Furthermore, the combined OSSE and OSO-8 data do not provide enough detail in the 20–60 keV range to rule out a break near 40 keV. The existence of a break in the energy range  $\sim 100$ – $200$  keV is likely, however, as noted by Ulmer (1993). This aspect of the spectral shape will be analyzed in detail in a future work that combines all the CGRO data. We also remark that it is just as likely that the spectral shape in the X-ray to gamma-ray range can be characterized by a spectrum that has a gradual change in slope (on a log-log plot) rather than by a set of discrete power laws joined together.

Knight (1982, 1983) also argued that the bridge spectrum is harder in the  $\sim 20$ – $100$  keV band than the peaks (see also Hasinger et al. 1982). But Mahoney et al. (1984) found no evidence for spectral variability across the pulse. As we have shown here, the spectral fitting does not reveal any differences across the pulse due to poor statistics. Our hardness ratio analysis does show that the bridge (and possibly peak 2) is indeed slightly harder than the first peak in the  $\sim 50$ – $110$  keV range (see results section), and that elsewhere in the

OSSE energy range ( $\sim 110\text{--}500$  keV), the bridge and peak 2 spectra are indistinguishable from the peak 1 spectrum. Given the weakness of the effect, however, the disagreement between our result and that of Mahoney et al. is not significant. Note that Knight's (1982) observations extended down to about 20 keV (about 30 keV lower than the OSSE or HEAO-3 C-1; Mahoney et al.). The spectral variation with phase in this lower energy range could be stronger than in the  $\sim 50\text{--}550$  keV energy range of the OSSE and HEAO-3 C-1.

Knight (1982) suggested the possibility that the bridge emission was thermal but later retracted that suggestion (Knight 1983). Due to the uncertainties in the models of pulsar emission, the variability of the pulse spectrum with phase cannot be used to distinguish between the following two models: (1) bridge emission that originates from a separate physical process/region of the neutron star; or (2) bridge emission that arises from the superposition of the emission beamed from the region(s) producing the peak emission.

A method for showing the energy dependence of the pulse shape was suggested by Hasinger (1984a). He made a plot of the ratio of the integrated flux values for the peak 2 combined with the bridge region to the integrated flux in P2. The definitions he used were the same as in Table 4 except that G. Hasinger (1993, private communication) included all the phase bins between peaks 1 and 2 in his definition of the bridge region. Here we reproduce the data from his Figure 2 (Figure 9) along with our own data for comparison. The figure clearly shows that the pulse shape is energy dependent.

Two other remarks are relevant: (1) There are also some  $\sim 3\sigma$  deviations in the hardness ratio versus phase (cf. Figure 5), which suggests that there may be some relatively rapid changes in spectra across the light curve. (2) Since the OSSE, EGRET (Nolan et al. 1993), optical, and X-ray light curves have significantly different pulse shapes (e.g., ratio of peak 1 versus peak 2, or bridge versus peaks, cf. Lyne & Graham-Smith 1990), it may not be appropriate to model average pulse spectra, but rather to model the individual regions. Perhaps theoretical emission models should really be compared at the various phases, as

suggested by Ho (1993), for example. Unfortunately, phase dependent predictions of the spectra are not yet available.

## 5. SUMMARY AND CONCLUSIONS

We have shown the following:

1. The phase of peak 1 and the radio agree to within  $\sim 30\mu s$ . This validates the combination of the CGRO clock system and the radio observations, which are quoted to an accuracy of  $300\mu s$ .
2. The phase of the peaks of the gamma-ray emission is independent of energy within the range of our measurements,  $\sim 50$ – $550$  keV.
3. There is no evidence for variability in the  $\sim 50$ – $340$  keV pulse intensity or shape on time scales from 2 minutes to 1 year. The  $3\sigma$  limits to the intensity of the pulse variations range from  $\lesssim 6\%$  (1 year) to  $180\%$  (2 minutes).
4. When we combine CGRO data with previously published work, we find evidence for a sinusoidal variation in the ratio of the peaks, with a  $\sim 13.1$  year periodicity. This period is consistent with the concept of precession.
5. If the precession model is correct, the optical emission from the Crab pulsar must have a markedly different beam profile than at higher energies since no evidence for this periodicity is seen in the optical data.
6. We cannot determine whether the radiation in the bridge region is a superposition of the beamed emission responsible for the two peaks in the light curve or emanates from a separate region. But, we have shown that the average light curve cannot be fit by a set of asymmetric Lorentzians. This is a geometrical model based upon the concept of bridge emission produced by superposing beams.

7. We see no evidence for lines in our spectra averaged over 1 week, and our limits are comparable to the fluxes of previously reported measurements. Transient line features can't be ruled out by the time averaged spectra. But none of the previous detections are at a level of significance that is in serious conflict with our upper limits.
8. The average spectrum probably has at least one break in the best-fit power law spectrum somewhere between 100 and 200 keV.
9. When the outer-gap model is fitted to the averaged pulsed spectrum from  $\sim 3$ –550 keV, the deviations of the model from the data are no larger than 10–20%, although the best fit produces a  $\chi^2$  that is unacceptably high ( $\chi^2 = 57$ , 24 degrees of freedom) due to the high statistical significance of our data.
10. Spectral fits do not reveal any statistically significant variation in the light curve with phase, but hardness ratio analysis does suggest that in the  $\sim 50$ –150 keV range the bridge spectrum is harder than the first peak at the 4–5  $\sigma$  level and is consistent with the hardness of the second peak. The effect of a harder bridge spectrum is likely to be stronger when the observations are extended down to  $\sim 20$  keV.

## 6. ACKNOWLEDGEMENTS

We thank the radio astronomers (Z. Arzoumanian, D. Nice, J. Taylor, S. Lundgren, and J. Cordes) for providing the data for the ephemerides. We thank C. Ho for providing the code for this outer-gap model, and we thank L. S. Finn for providing us with a theoretical discussion of the neutron star precession. We thank the *CGRO* flight operations team led by B. Breshears for providing us with a stable and accurate clock. We also thank the referee, G. Hasinger, for very useful comments. This work was supported in part by NASA grant DPR S-10987C.

Table 1: Summary of OSSE Configurations

Observation date (TJD)	Precision	Energy Ranges (MeV)
8373–8374	1 ms	0.090–0.15, 0.27–0.50
8374–8377	1/8 ms	0.11–0.15, 2.4–10.0
8393–8400	1 ms	0.06–0.30, 2.0–10.0
8400–8406	1 ms	0.35–1.15, 2.0–10.0
8798–8804	1 ms	0.090–0.14, 0.35–0.54

Table 2: Crab pulsar ephemeris

TJD Span	8371–8412	8794–8816
$\nu$	$29.9492515379593 \text{ s}^{-1}$	$29.9350985720614 \text{ s}^{-1}$
$\dot{\nu}$	$-3.77657 \times 10^{-10} \text{ s}^{-2}$	$-3.77229 \times 10^{-10} \text{ s}^{-2}$
$\ddot{\nu}$	$8.18 \times 10^{-21} \text{ s}^{-3}$	$1.17 \times 10^{-20} \text{ s}^{-3}$
$T_{0geo}$	8371.000000104 (TJD)	8805.000000153 (TJD)
RA(J2000)	$5^{\text{h}}34^{\text{m}}31^{\text{s}}.973$	--
Dec(J2000)	$22^{\circ}00'52''.06$	--
DM	$56.776^a(5) \text{ ms}$	$56.790(5) \text{ ms}$

a. S. Lundgren & J. Cordes 1991, private communication.

Table 3: Limits to time variability of the OSSE light curve

Time scale	Observation period (TJD)	Energy range (keV)	# fitted subpulses	$3\sigma^a$ (%)
2 minutes	8394–8399	50–340	877	180
1.5 hours	”	”	88	50
1 day	”	”	7	10
3 weeks	8373–8399 <sup>b</sup>	95–133	1	6
1 year	8373–8805 <sup>c</sup>	95–140	1	7

Notes for Table 3

a. upper limit to variability of total intensity of pulsed emission

b. 8373–8377 vs. 8393–8399

c. 8394–8399 vs. 8798–8804

Table 4: Definition of phase intervals of the Crab pulsar

Region	Phase interval
Peak 1	0.95–0.05
Bridge	0.08–0.27
Peak 2	0.30–0.44
Background	0.60–0.80
Total composite pulse	0.85–0.55

Table 5: Power law fits to spectra of the profile components

Region	Intensity*	Index	$\chi^2/\nu^\dagger$
Peak 1	$0.012 \pm 0.0006$	$-2.07 \pm 0.03$	1.14
Bridge	$0.0096 \pm 0.0005$	$-1.93 \pm 0.05$	1.05
Peak 2	$0.020 \pm 0.001$	$-2.00 \pm 0.03$	1.13
Total	$0.050 \pm 0.003$	$-1.99 \pm 0.03$	1.04

\* Flux = Intensity  $\times$  (E/.130 MeV) $^\alpha$  photons cm $^{-2}$  s $^{-1}$  MeV $^{-1}$ , where  $\alpha$  = Index phase averaged, see text

$^\dagger$  648 degrees of freedom.

Table 6: Broken Power law fits to spectra of the profile components

Region	Intensity*	Break Energy <sup>†</sup>	Index 1	Index 2	$\chi^2/\nu^\ddagger$
Peak 1	0.020	0.104	−1.18	−2.35	1.10
Bridge	0.014	0.116	−1.56	−2.16	1.04
Peak 2	0.017	0.149	−1.73	−2.41	1.03
Total	0.07	0.118	−1.67	−2.25	1.01

\* Flux = Intensity  $\times$  (E/Break Energy) $^\alpha$  photons cm $^{-2}$  s $^{-1}$  MeV $^{-1}$ , where  $\alpha$  = Index 1 for energies below the break energy, and  $\alpha$  = Index 2 for energies above the break energy.

<sup>†</sup> The energy where the two powers join, in MeV.

<sup>‡</sup> 646 degrees of freedom.

Table 7: Upper limits ( $3\sigma$ ) for time integrated lines

E (keV)	Total $10^{-3}$ photons $\text{cm}^{-2} \text{s}^{-1}$	Bridge	Peak 1	Peak 2	Previous Detections <sup>a</sup>	Ref. <sup>b</sup>	Previous Limits <sup>e</sup>	Ref. <sup>c</sup>	Comments <sup>f</sup>
73	0.30	0.30	0.19	0.24	$3.8 \pm 0.9$	1	2, 1, 0.3	8, 9	unpulsed
78	0.51	0.32	0.15	0.17	$3.0 \pm 0.9$	2, 3 <sup>d</sup>	1.9, 0.7	9, 10	25 min (ref 2)
					$5.0 \pm 1.5$				unpulsed (ref 3)
400	0.57	0.19	0.085	0.13	$2.24 \pm 0.65$	4, 5	1.7; 0.18	9, 11, 12	
					$7.4 \pm 2.1$				
440	0.50	0.12	0.078	0.11	$0.086 \pm 0.033$	6	0.3	9	bridge only
511	0.47	0.11	0.036	0.12			0.3	9	
545	0.14	0.12	0.043	0.05	$4.5 \pm 1.2$	7 <sup>d</sup>	0.3	9	unpulsed 24 hrs.

Notes for Table 7

a)  $10^{-3}$  photons  $\text{cm}^{-2} \text{s}^{-1}$ , phase averaged; see text and Table 4 for definitions

b) References for previous detections

c) References for previous upper limits

d) Based on total Crab nebula plus pulsar spectrum

e) Upper limits ( $3\sigma$ )

f) Comments related to previous detections.

References: 1. Ling et al. 1979, 2. Strickman et al. 1979, 3. Manchanda et al. 1982,

4. Leventhal et al. 1977, 5. Ayre et al. 1983, 6. Massaro et al. 1991,

7. Gilfanov et al. 1994, 8. Schwartz et al. 1980,

9. Mahoney et al. 1984 (including analysis of previous work), 10. Hasinger et al. 1982,

11. Ling et al. 1977, 12. Hameury et al. 1983

## REFERENCES

- Agrinier, B., et al. 1990, *ApJ*, 355, 645
- Arons, J. 1983a, in *Positron-Electron Pairs in Astrophysics*, ed. M. L. Burns, A. K. Harding, & R. Ramaty (New York: AIP), 163
- Arons, J. 1983b, *ApJ*, 266, 215
- Arons, J. 1984, *Adv. Space Res.*, 3 (10–12), 287
- Arzoumanian, Z., Nice, D., & Taylor, J. H. 1992. *GRO/Radio Timing Database*. Princeton Univ.
- Avni, Y. 1976, *ApJ*, 210, 642
- Ayre, C. A., Bhat, P. N., Ma, Y. Q., Myers, R. M., & Thompson, M. G. 1983, *MNRAS*, 205, 285
- Brecher, K., & Ulmer, M. P. 1978, *Nature*, 271, 135
- Cheng, K. S., Ho, C., & Ruderman, M. 1986a, *ApJ*, 300, 500
- Cheng, K. S., Ho, C., & Ruderman, M. 1986b, *ApJ*, 300, 522
- Chiang, J., & Romani, R. W. 1993, in *Isolated Pulsars: Proc. of the Los Alamos Workshop*, ed. K. A. Van Riper, R. Epstein, & C. Ho (Cambridge: Cambridge Univ. Press), 287
- Clear, J., Bennett, K., Buccheri, R., Grenier, I. A., Hermsen, W., Mayer-Hasselwander, H. A., & Sacco, B. 1987, *A&A*, 174, 85
- Daugherty, J. K., & Harding, A. K. 1982, *ApJ*, 252, 337
- Fritz, G., Meekins, J. F., Chubb, T. A., Friedman, H., & Henry, R. C. 1971, *ApJ*, 164, L55
- Gilfanov, M., et al. 1994, *ApJS*, 92, 411

- Hameury, J. M., Boclet, D., Durouchoux, P., Cline, T. L., Paciesas, W. S., Teegarden, B. J., Tueller, J., & Haymes, R. C. 1983, *ApJ*, 270, 144
- Hasinger, G. 1984a, in *The Crab Nebula and Related Supernova Remnants*, ed. M. Kafatos & R. B. Henry (Garching: Cambridge Univ. Press), 43
- Hasinger, G. 1984b, Ph.D. thesis, Ludwigs-Maximilians-Univ.
- Hasinger, G., Pietsch, W., Reppin, C., Trümper, J., Voges, W., Kendziorra, E., & Staubert, R. 1982, in *Accreting Neutron Stars*, ed. W. Brinkmann & J. Trümper (Garching: Max-Planck-Institut), 130
- Hasinger, G., Pietsch, W., Reppin, C., Trümper, J., Voges, W., Kendziorra, E., & Staubert, R. 1984, *Adv. Space Res.*, 3 (10–12), 63
- Ho, C. 1989, *ApJ*, 342, 396
- Ho, C. 1993, in *Isolated Pulsars: Proc. of the Los Alamos Workshop*, ed. K. A. Van Riper, R. Epstein, & C. Ho (Cambridge: Cambridge Univ. Press), 271
- Johnson, W. N., et al. 1993, *ApJS*, 86, 693
- Jones, D. H. P., Smith, F. G., & Nelson, J. E. 1980, *Nature*, 283, 50
- Kanbach, G. 1990, in *The Energetic Gamma-Ray Experiment Telescope (EGRET) Science Symposium*, ed. C. Fichtel et al. (Washington, DC: NASA), 101
- Knight, F. K. 1982, *ApJ*, 260, 538
- Knight, F. K. 1983, in *Positron-Electron Pairs in Astrophysics*, ed. M. L. Burns, A. K. Harding, & R. Ramaty (New York: AIP), 141
- Kristian, J. 1971, in *The Crab Nebula*, ed. R. D. Davies & F. G. Smith (Dordrecht: Reidel), 87

- Kurfess, J. D. 1971, *ApJ*, 168, L39
- Leventhal, M., MacCallum, C. J., & Watts, A. C. 1977, *Nature*, 266, 696
- Ling, J. C., Mahoney, W. A., Willett, J. B., & Jacobson, A. S. 1977, *Nature*, 270, 36
- Ling, J. C., Mahoney, W. A., Willett, J. B., & Jacobson, A. S. 1979, *ApJ*, 231, 896
- Lundgren, S. C., et al. 1994, in preparation
- Lundgren, S. C., Cordes, J. M., Foster, R., Hankins, T., Ulmer, M. P., & Garasi, C. 1992, in *The Compton Observatory Science Workshop*, ed. C. Shrader, N. Gehrels, & B. Dennis (Washington, DC: NASA), 260
- Lyne, A. G., & Graham-Smith, F. 1990, *Pulsar Astronomy* (Cambridge: Cambridge Univ. Press)
- Mahoney, W. A., Ling, J. C., & Jacobson, A. S. 1984, *ApJ*, 278, 784
- Manchanda, R. K., Bazzano, A., La Padula, C. D., Polcaro, V. F., & Ubertini, P. 1982, *ApJ*, 252, 172
- Massaro, E., et al. 1992, in *The Compton Observatory Science Workshop*, ed. C. Shrader, N. Gehrels, & B. Dennis (Washington, DC: NASA), 222
- Massaro, E., et al. 1991, *ApJ*, 376, L11
- Nolan, P. L., et al. 1993, *ApJ*, 409, 697
- Ögelman, H., Finley, J. P., & Zimmermann, H. U. 1993, *Nature*, 361, 136
- Pravdo, S. H., & Serlemitsos, P. J. 1981, *ApJ*, 246, 484
- Schwartz, R., Lin, R. P., Pelling, R., & Hurley, K. 1980, *BAAS*, 12 (2), 542
- Strickman, M. S., Johnson, W. N., & Kurfess, J. D. 1979, *ApJ*, 230, L15

Taylor, J. H., & Weisberg, J. M. 1989, *ApJ*, 345, 434

Toor, A., & Seward, F. D. 1977, *ApJ*, 216, 560

Ulmer, M. P. 1993, *ApJS*, 84, 789

Ulmer, M. P., et al. 1993, *ApJ*, 417, 738

Walraven, G. D., Hall, R. D., Meegan, C. A., Coleman, P. L., Shelton, D. H., & Haymes, R. C. 1975, *ApJ*, 202, 502

Wills, R. D., et al. 1982, *Nature*, 296, 723

## 7. FIGURE CAPTIONS

Figure 1. Crab light curve from the OSSE data produced with data time tagged to 1/8 ms precision.

Figure 2. Crab light curves from the OSSE data at various energies, produced with data time tagged to 1 ms precision. The vertical dashed lines show the definitions of the background (B), peak 1 (P1), the bridge (Br), and peak 2 (P2), as used later for measuring spectra.

Figure 3. Top panel shows the phase of peak 1 relative to the phase of the radio; the bottom

panel shows the relative separation of peak 1 to peak 2. The dashed horizontal lines are best-fit values. The uncertainties shown are only statistical (see text).

Figure 4. (a) is the spectrum of peak 1, (b) spectrum of the bridge, (c) spectrum of peak 2 (see Figure 2 for phase definitions of each region). The dashed lines are the best-fit single power law, the solid lines are the best-fit broken power laws (see text). Upper limits ( $2\sigma$  above 0) are plotted for intensity values which were found to be less than  $1\sigma$  above zero.

Figure 5. The best-fit spectral index to a single power law as a function of phase. The same convention for upper limits as in Figure 4 was used.

Figure 6. The hardness ratios as a function of phase along with the average light curve are shown. The definitions of the peaks and bridge are also displayed for reference.

Figure 7. The ratio of peak 2 to peak 1 ( $P2/P1$ ) versus time. The upper curve is for the  $\sim 50$ – $500$  keV range and the lower curve is for the  $\gtrsim 50$  MeV range. The dot-dashed horizontal lines are the mid-ranges of the respective best-fit sine waves; the dashed lines show the best-fit constant.

Figure 8. The OSSE data combined with the lower energy data from NRL (Fritz et al. 1971), LLL (Toor & Seward 1977), and OSO-8 (Pravdo & Serlemitsos 1981). The solid line is the best-fit broken power law, the dashed line is the best-fit single power law and the dot-dashed line is the outer-gap model of Ho (1989, 1993). The single upper limit is  $3\sigma$ . The asterisk denotes OSSE data; the filled diamond, OSO-8; the open triangle, LLL; and the open square, NRL. The best fits are to the OSO-8 and OSSE data alone. The other

data sets are included to demonstrate that they are also consistent with a broken power law (see text). The same convention for upper limits as in Figure 4 was used.

Figure 9. The ratio of the peak 2 plus bridge to peak 1 as a function of energy. The OSSE data are plotted with asterisks, the rest of the data are from Hasinger (1984a) and references therein.

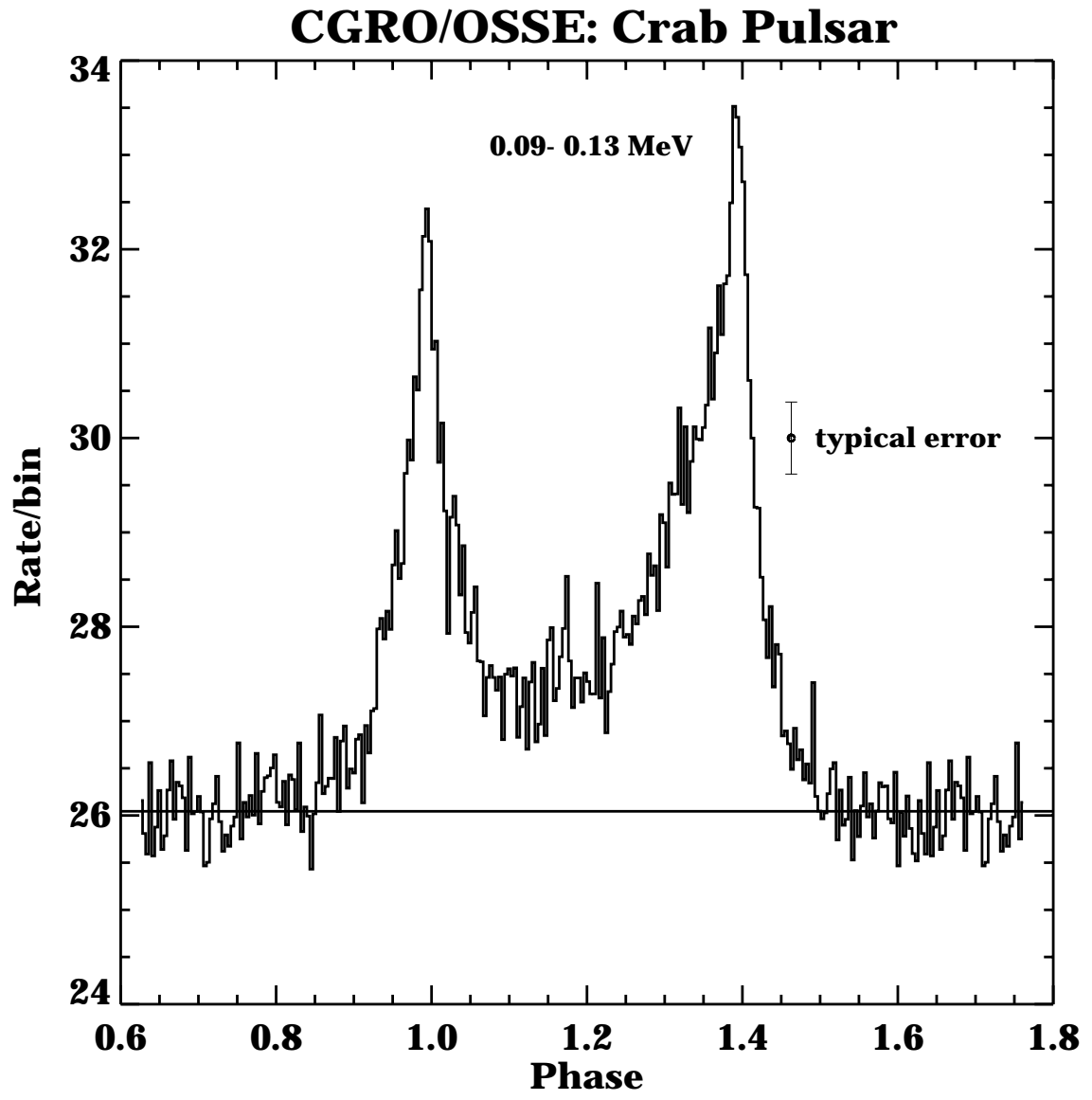


Fig. 1.—

## OSSE: Crab Pulsar

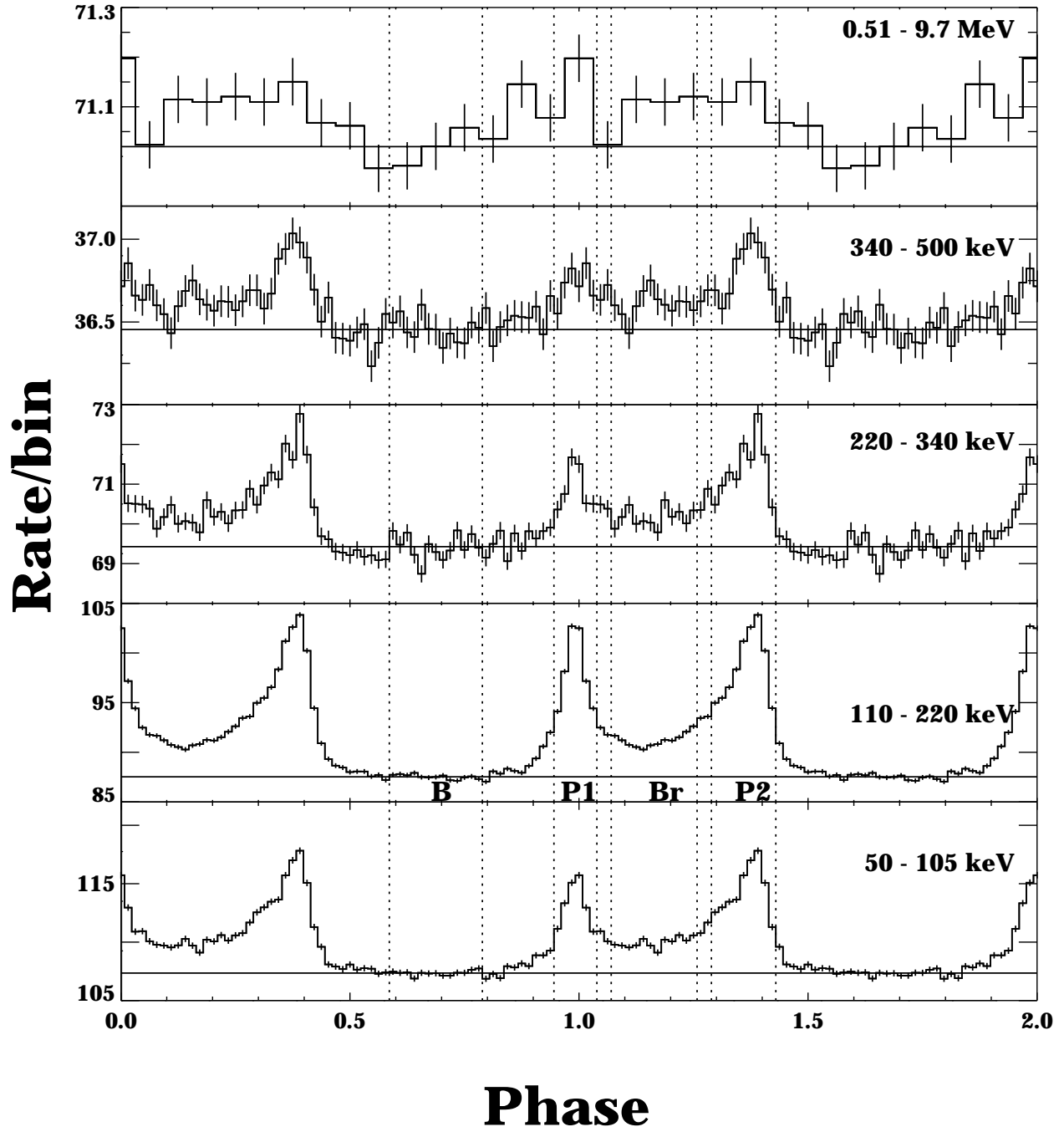


Fig. 2.—

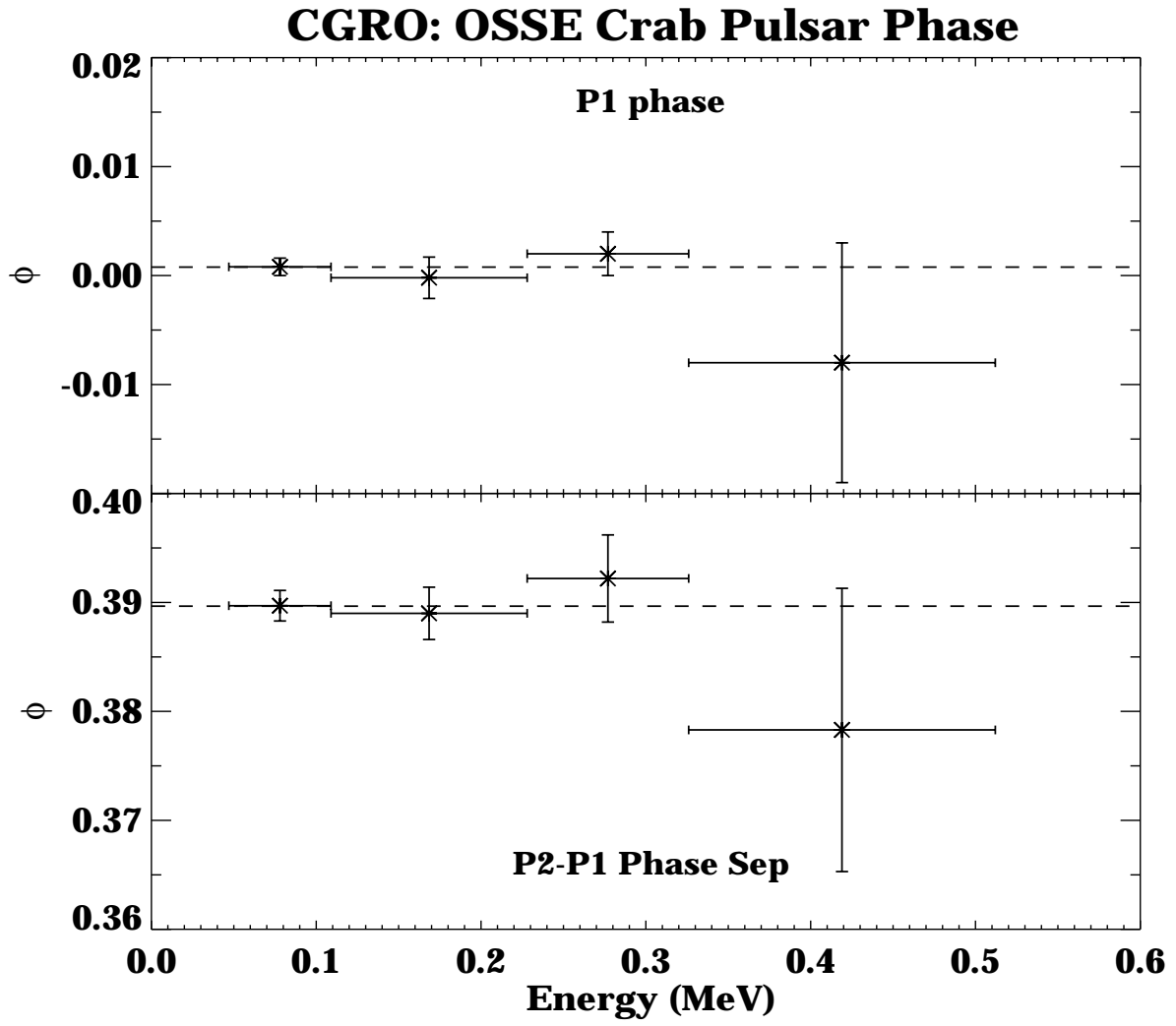


Fig. 3.—

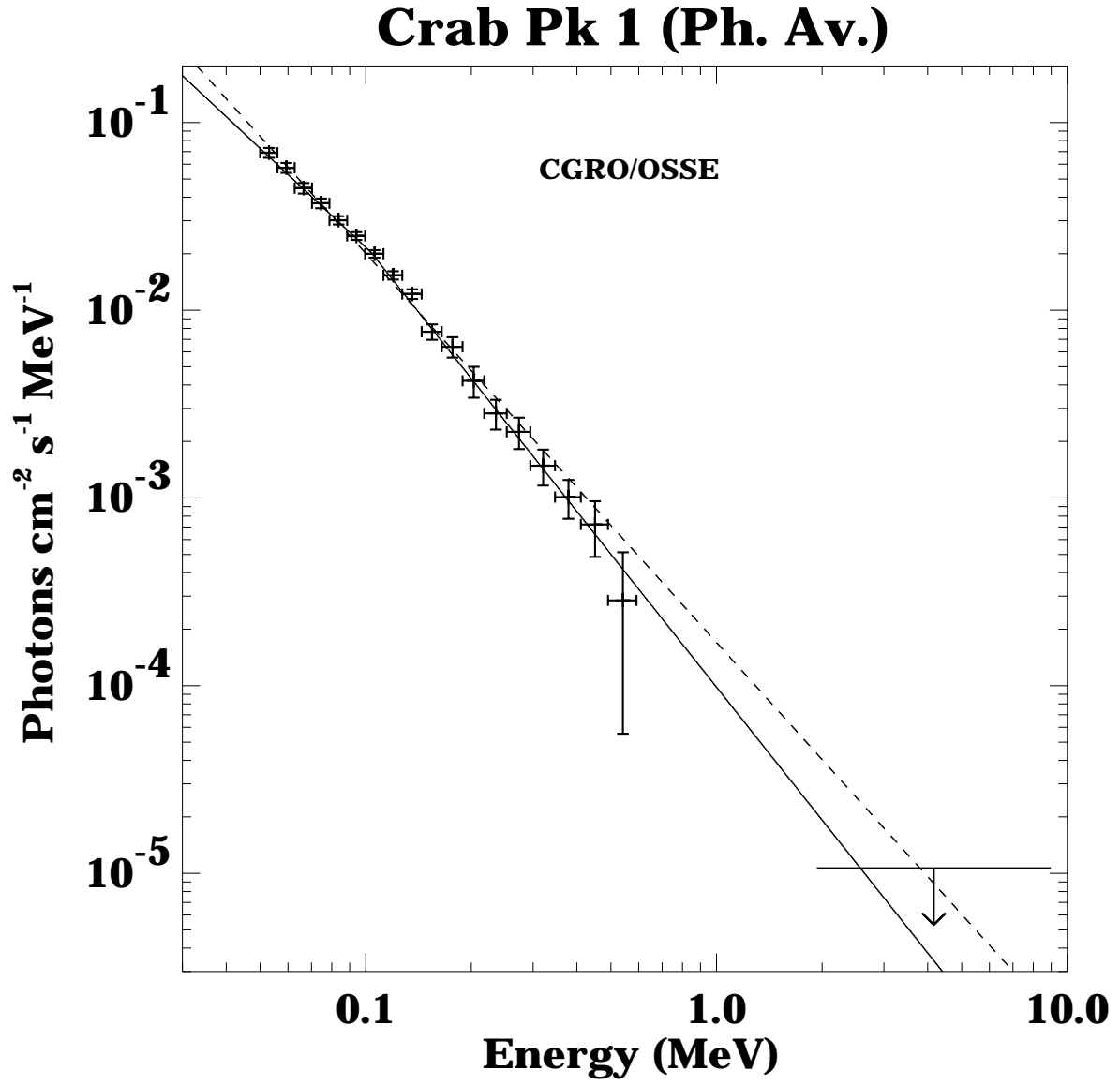


Fig. 4.— a

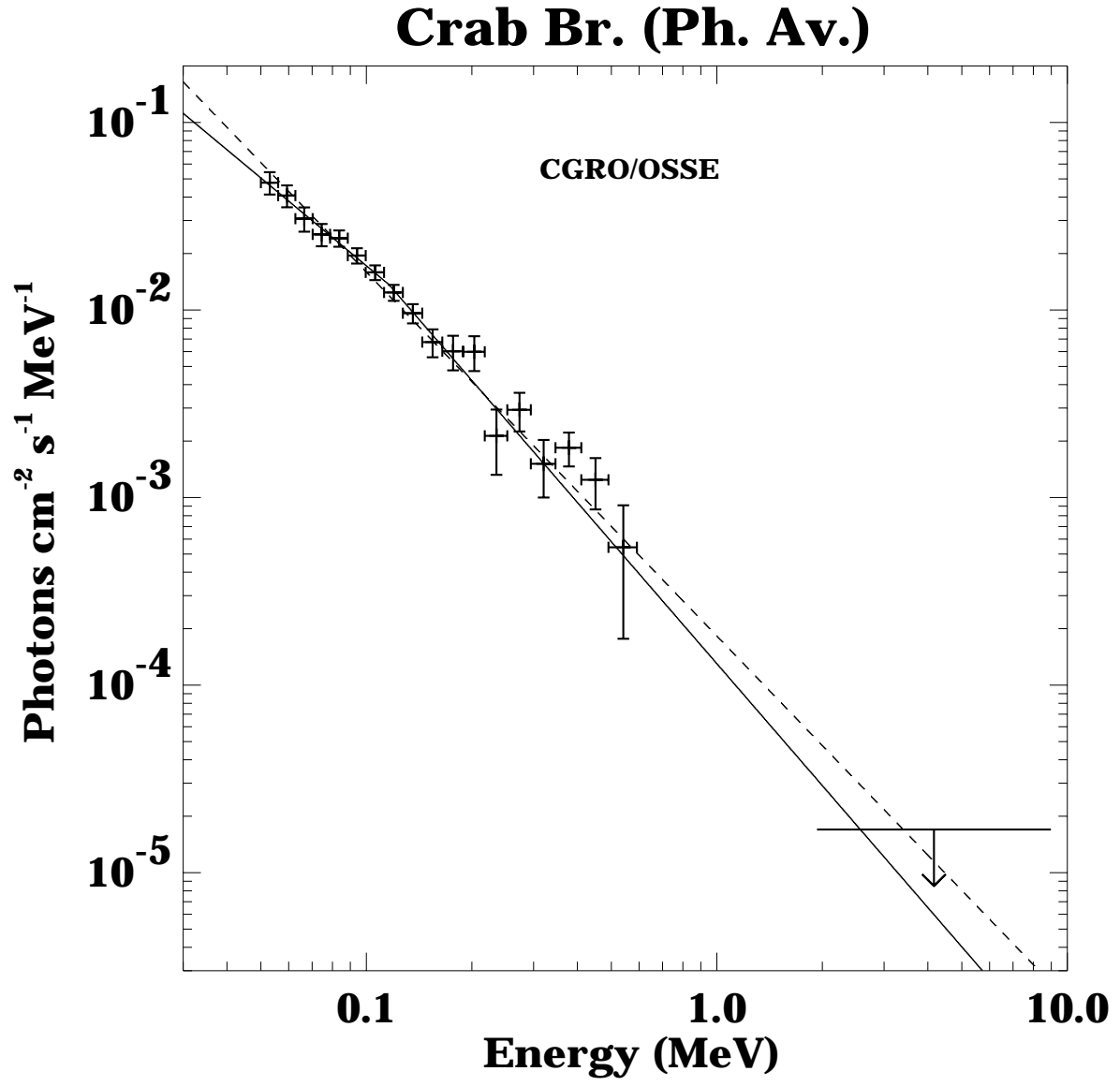


Fig. 4.— b

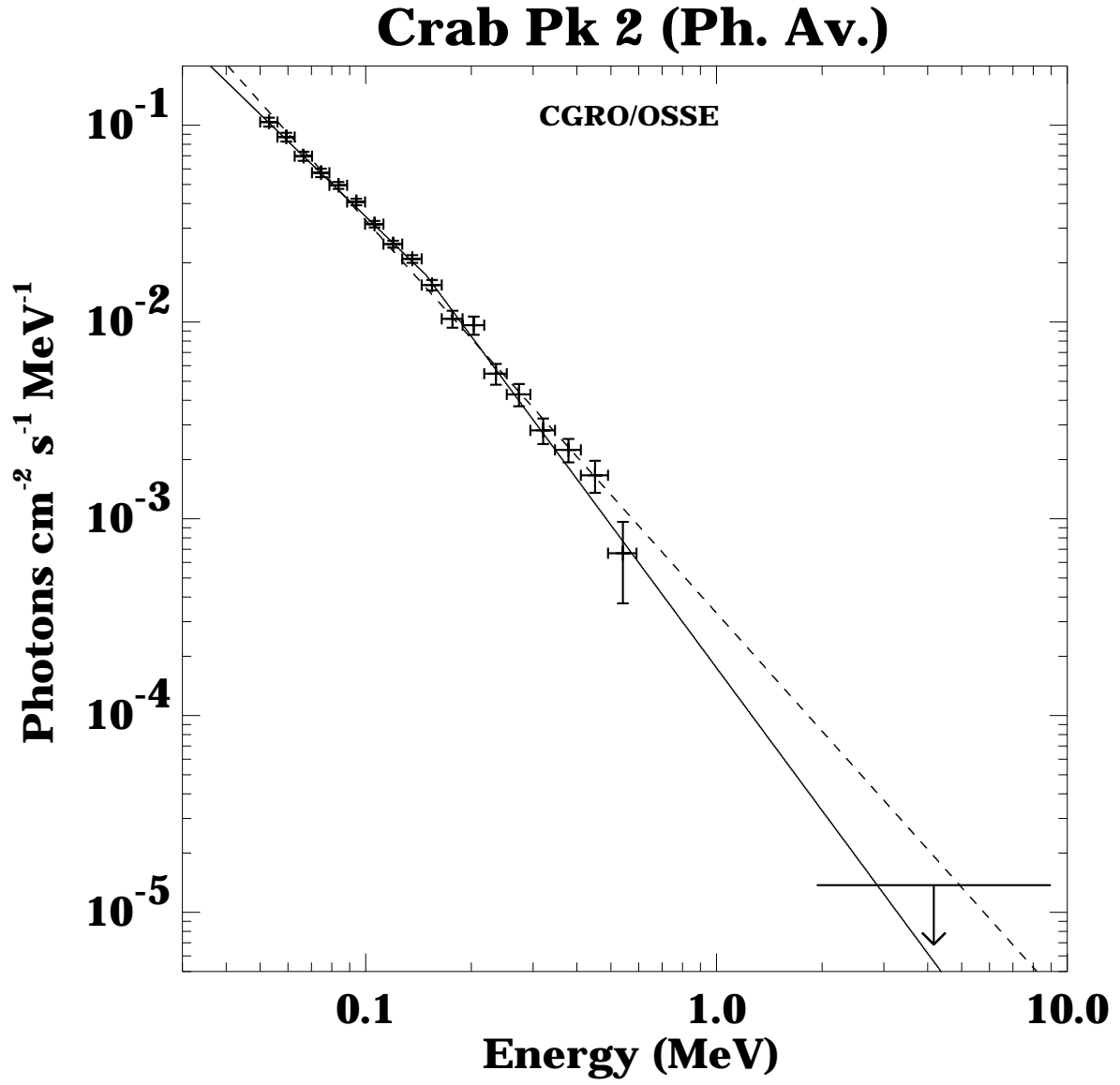


Fig. 4.— c

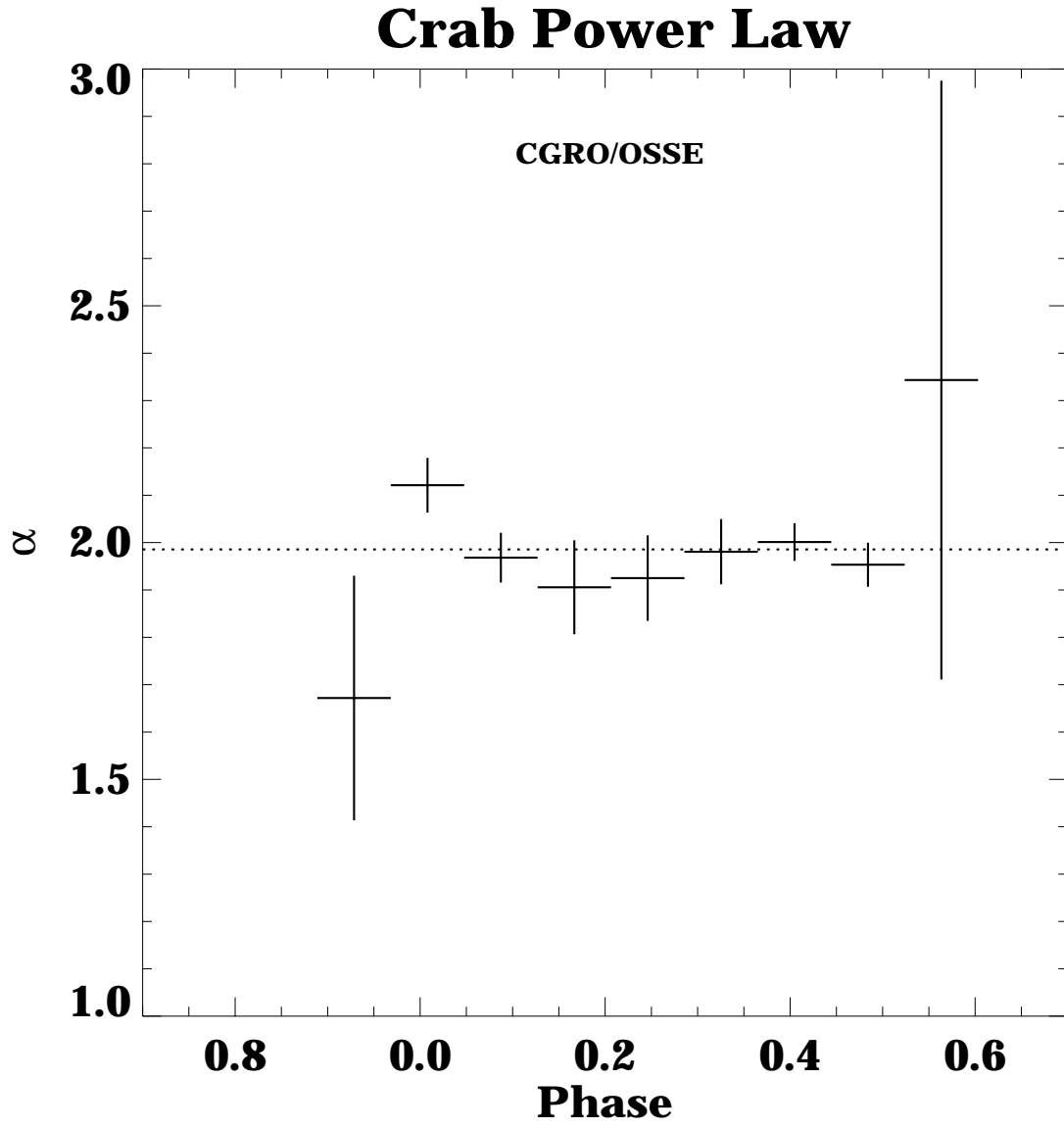


Fig. 5.—

# OSSE: Crab Pulsar

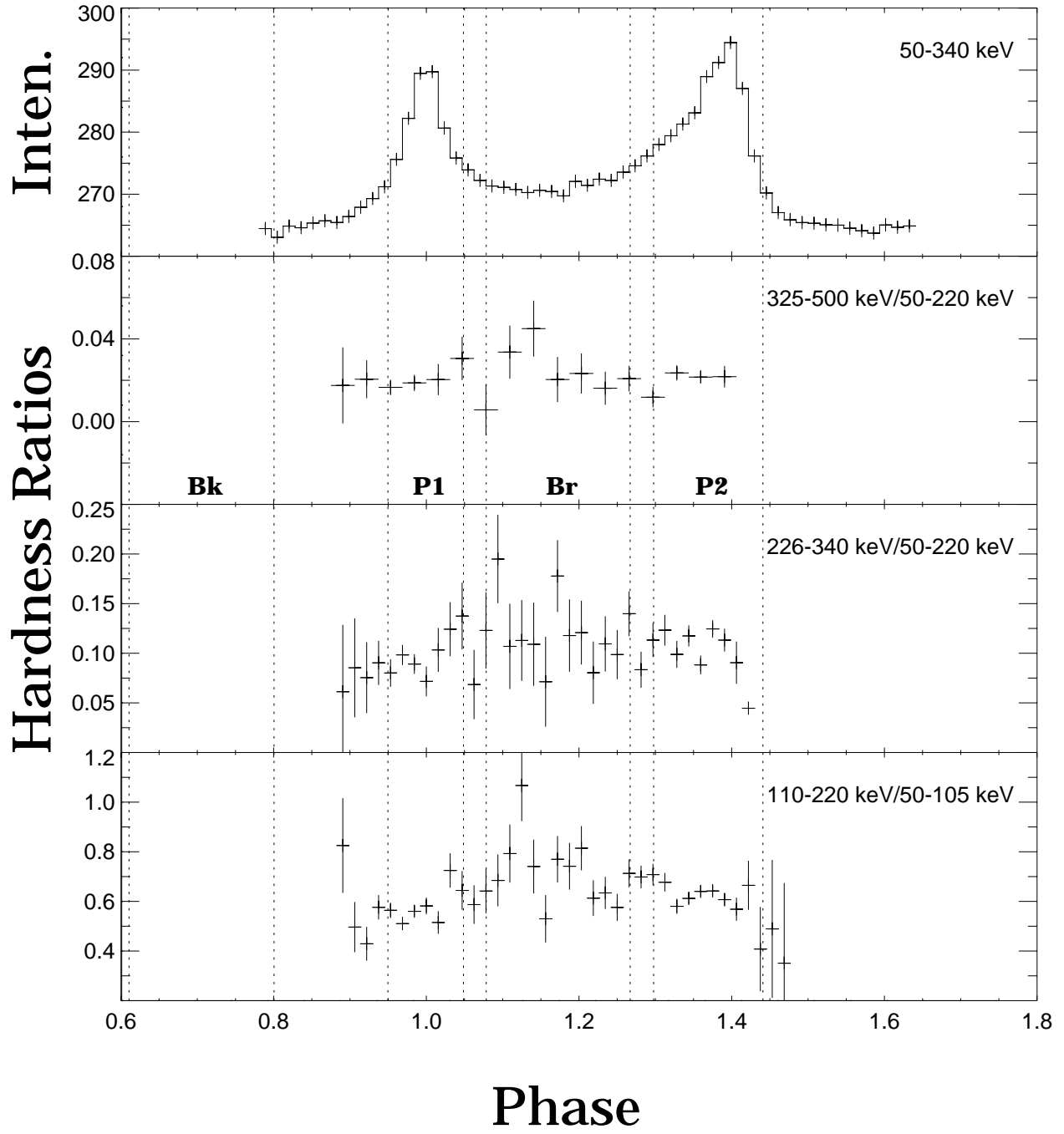
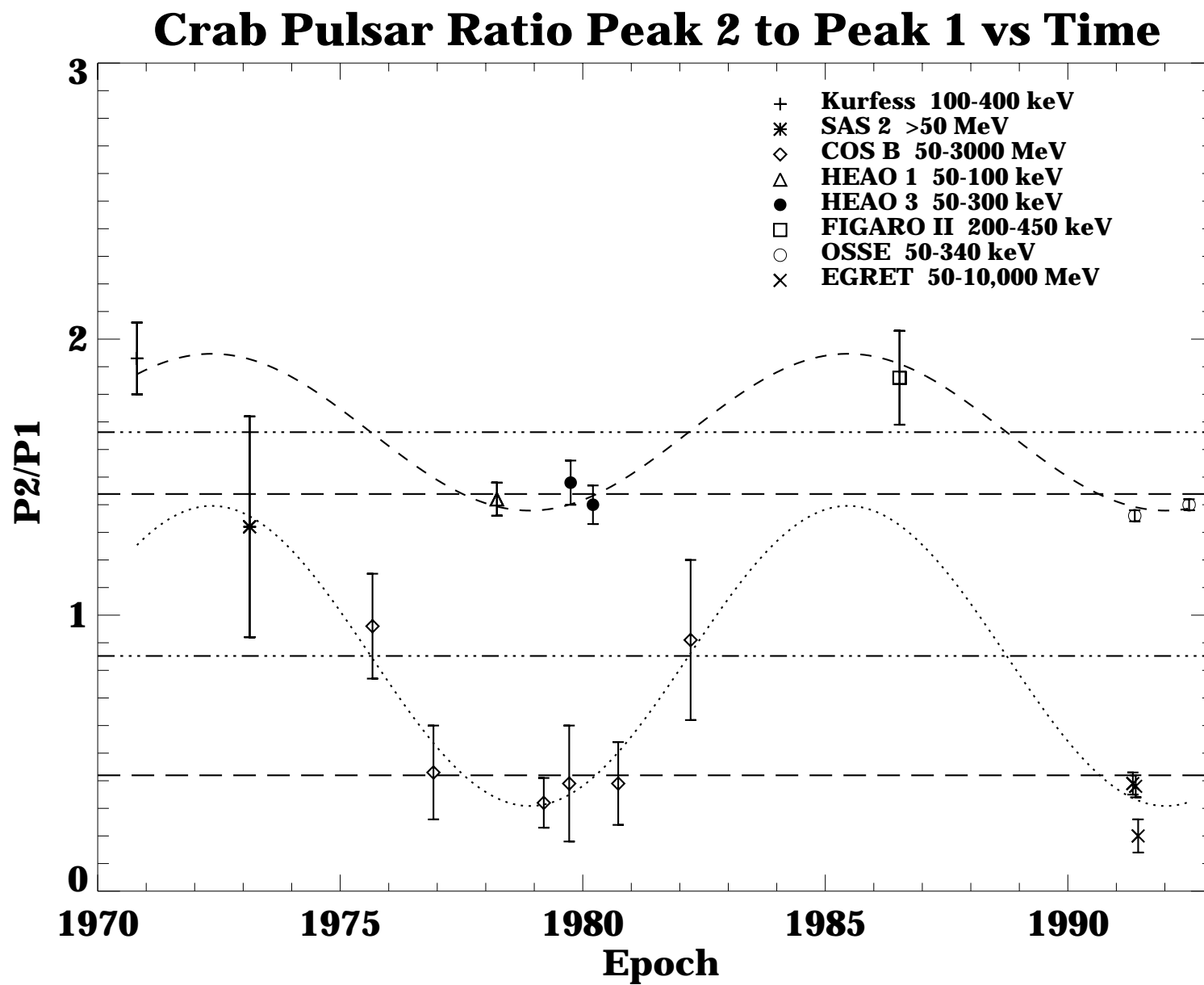
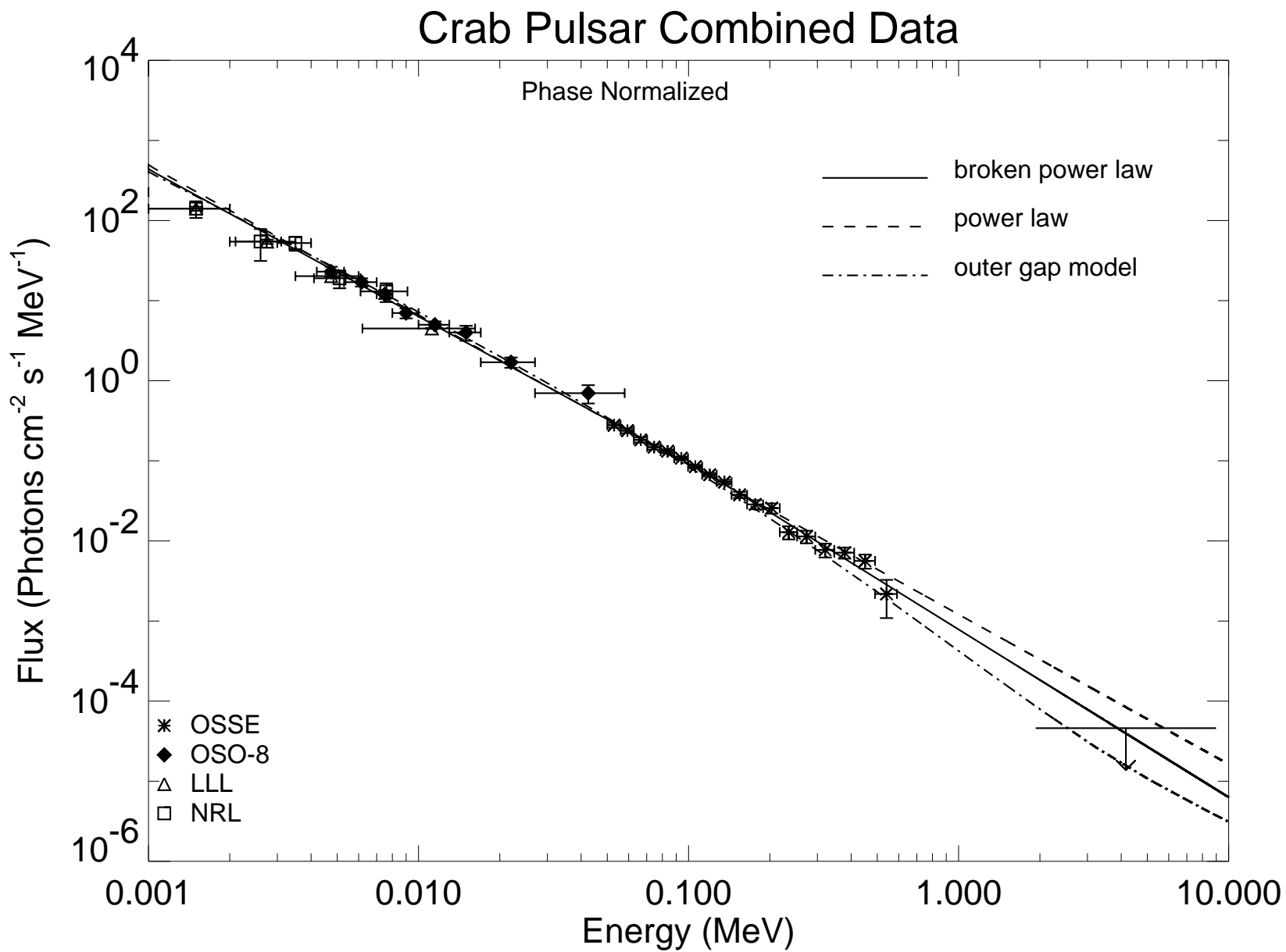


Fig. 6.—

Fig. 7.—





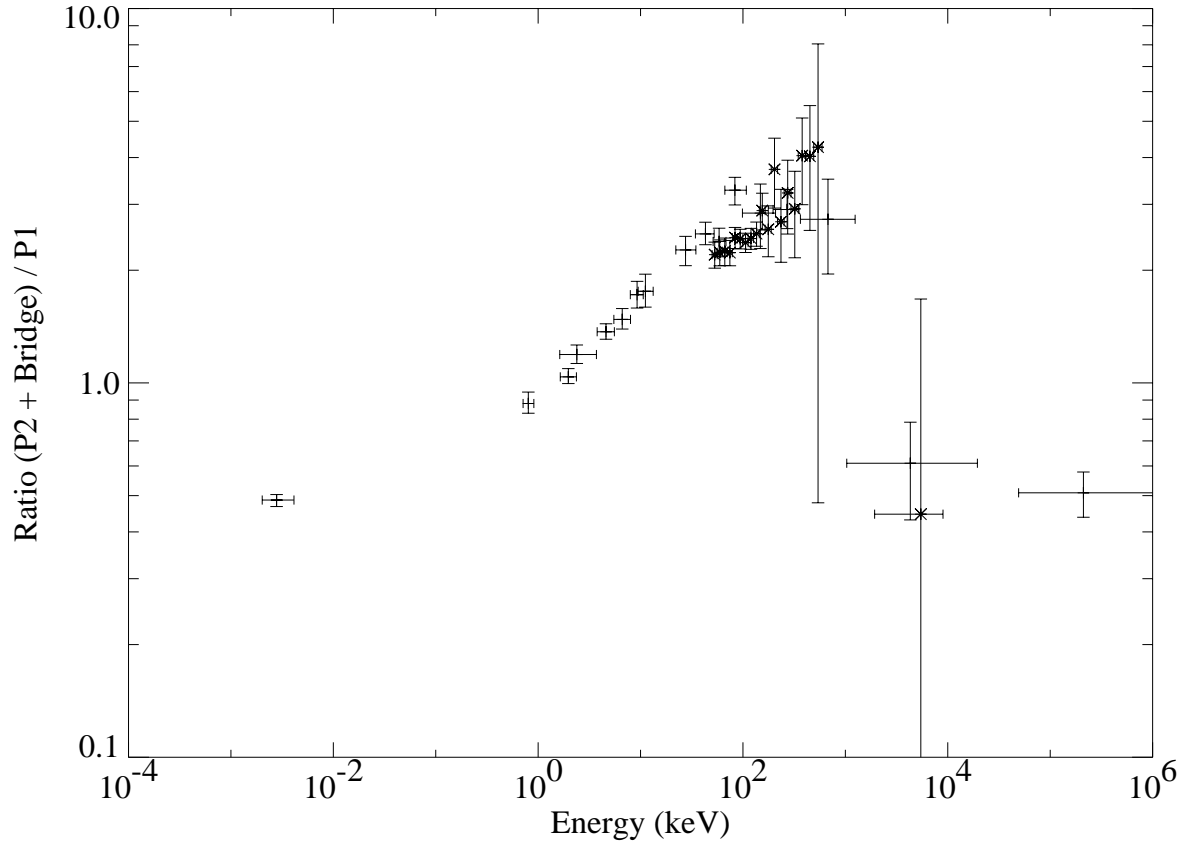


Fig. 9.—